Hindawi
Geofluids
Volume 2022, Article ID 9410466, 12 pages
https://doi.org/10.1155/2022/9410466

Research Article

Study on the *In Situ* Test of the Treatment Effect for the Riverbank Soft Soil Subgrade in the Hetao Area

Shen Zuo,[1] Tian-yu Li,[1] Peng Jiang,[2] Xiang-long Zuo,[1] and Jin Li[1]

[1]*School of Civil Engineering, Shandong Jiaotong University, Jinan 250357, China*
[2]*School of Civil Engineering, Shandong University, Jinan 250061, China*

Correspondence should be addressed to Peng Jiang; jiangp2020@mail.sdu.edu.cn and Jin Li; lijinsdjtu@163.com

Received 6 May 2022; Revised 9 June 2022; Accepted 21 June 2022; Published 30 July 2022

Academic Editor: Dongjiang Pan

The Inner Mongolia Hetao area has a widely distributed riverbank fluvial soft soil with high groundwater levels and ground surface water. This situation may incur some potential engineering problems for the Linhe-Baigeda section of the Beijing-Xinjiang Expressway, such as subgrade settlement control and waterproofing. *In situ* experiments were conducted on the site using five subgrade base treatment schemes for subgrade construction. The long-term monitoring of various technical indicators like settlement, earth pressure, pore water pressure, and reinforcement material deformation was carried out. Study results show that the cumulative settlement generated when the double-layer geogrid reinforces the subgrade base is 6.9 cm, which is the smallest among the five subgrade base reinforcement methods, and the cumulative settlement of the subgrade base reinforced with a single-layer geocell is the largest, which is 15.4 mm. The size and distribution of subgrade earth pressure change significantly during farmland irrigation. When the single-layer geocell reinforces the base, the subgrade stress is smaller than that of the other four, and the average earth pressure is 8 kPa. The membrane-pulling effect of reinforcement material significantly disperses the upper load of subgrade backfill soil, and the subgrade settlement control with different base treatment schemes meets the technical requirements.

1. Introduction

The Hetao area of the Inner Mongolia Autonomous Region is located in the Yellow River alluvial plain, with a large area of well-distributed fluvial soft soil. The soil is characterized by common soft soil, like high water content, large pore ratio, and low strength. Some unique engineering geology is also presented in this area, such as the soft soil interbeds with uneven stratification of sand and peat, irregularly distributed with zonal or lenticular shape. Besides, farmland is widely distributed in this area. With a large quantity of irrigation channels, the surface flooding irrigation form is adopted. As a result, large areas of surface soil dipped in the water for a long time, which incurs seasonal water accumulation in the ground, wet shoal, humus and mucky soil, and soil liquefaction or salinization [1–4].

The construction of roads in the Hetao area of Inner Mongolia plays an important role in serving the public and promoting economic development [5, 6]. As mentioned above, during the highway subgrade construction on the soft soil ground of the Hetao area, the problems of high groundwater levels, poor ground bearing capacity, and seasonal flooding are inevitable. The National Highway 110 sections at Wuhai city of Inner Mongolia appeared to have subgrade diseases, such as mud pumping, as well as frost heaving and thawing settlement, under the capillary action of ground surface water [7]. Uneven settlement and sinking of the Baolan Railway subgrade were incurred by rising groundwater and surface water. The 10-25 mm of subgrade settlement in one single day resulted in a 66-day delay for railway transportation [8].

It can be seen that choosing applicable, economical, and effective treatment technology for subgrade construction in this area is of importance. The effective treatment methods include the ground replacement method [9, 10], addition agent solidification method [11–15], chemical grouting method [16–19], and freezing method [20–24]. Ou et al. [25] established optimal combination forecasting models to

calculate the settlement of the soft ground in a desert area, which reaches a more accurate result. Yang [26] studied the characteristics of eolian sand of the Hetao area; the eolian sand cushion replacement technology is employed and studied with numeral simulation. Shan et al. [27] established a numerical model of the block-stone embankment in Inner Mongolia and investigated the water content, temperature, and deformation conditions of the subgrade.

The engineering practice in the region shows that the reinforced subgrade constructed with suitable backfill soil on the hard shell of the soft ground surface could achieve an excellent control effect of postconstruction settlement [28–35]. However, the traditional subgrade reinforcement treatment schemes mostly use geogrids and geocells, and there is insufficient data on *in situ* reinforcement treatment for the soft soil subgrade in the Hetao area. There is also no research on the reasonable reinforcement method for the Hetao Irrigation District. In addition, the influence of the groundwater level and the seasonal fluctuation of surface water on the soil pressure of the soft foundation is not clear.

Therefore, a long-term *in situ* test (for one year) was conducted by setting up different subgrade base treatment test sections. Based on the experimental data, the reinforcement effect and stress deformation distribution of different treatment types of the subgrade base are analyzed, and comprehensively considering economic, engineering, and other factors to select the optimal treatment plan, it provides a scientific basis for the future construction of expressways in the Hetao Irrigation District and further improvement of the research system of the treatment technology of the subgrade base.

2. Engineering Situation

2.1. Geological Condition. The Jingxin Expressway is an indispensable component of the sixth ray of the national expressway network, and the format of 4 bidirectional lanes is adopted for the main line with a design speed of 100 km/h, an integral roadbed. Located in the western part of Inner Mongolia Bayannur city, the Linhe-Baigeda section of the Jingxin Expressway is 58.986 km long. Bayannur is located in the Hetao area of the Yellow River alluvial plain, which is characterized by fluvial soft soil. The stratigraphic characteristics include the following:

(1) Holocene alluvial-diluvial deposits (Q4al+PL), where the main components are silty sand, fine sand, and medium sand, mostly present as yellow-brown, loose-dense, and slightly wet-saturated, and part of the surface layer is distributed with thinner dark gray and black silt

(2) Holocene eolian deposits (Q4eol), where the main components are fine sand, mostly present as yellow-gray and brown-yellow, slightly dense-dense, and dry-slightly wet, and the interlayer of thin silty clay partially exists

In addition to the poor geological condition, the problems of subgrade flooding also need to be considered during the irrigation period. Due to the surface flooding irrigation, water accumulation of the ground surface in some sections is sometimes as deep as 0.5~1 m for a long time, as shown in Figure 1.

Table 1 shows the physical and mechanical properties of the ground soil of the poor geological sections. The schematic diagram of the soil borrowing position is shown in Figure 2.

2.2. Treatment Scheme. In view of the available treatment options and the special local circumstances, according to the overall design principle of safe, reliable, economical, reasonable, and efficient construction, the selections of project treatment schemes are as follows:

(1) Sand and gravel cushion replacement is adopted for the sections with better drainage conditions

(2) When the thickness of the hard shell layer is greater than 1 m, the reinforced sand cushion can be used

(3) The block-stone replacement or geocell-reinforced gravel cushion can be employed for the soft soil ground in a small scope or sections that are not part of the main structure

Considering the experimental requirements and the progress of site construction, the total length of the test section is 500 m, and five base treatment methods with each 100 m test section are adopted, respectively. The experimental scheme is designed and set as follows in Table 2.

2.3. In Situ Test Procedure. The objectives of this study are to observe the deformation law of the subgrade and consolidation law of the soft ground, analyze the distribution and variation of base earth pressure, and figure out the seasonal change law of groundwater levels. The newly built subgrade is subjected to long-term monitoring of different base treatment schemes. The total amount of embedded components in the test section is shown in Table 3.

Test components and instruments are as follows: settlement plate, layered settlement magnetic ring, flexible displacement meter, earth pressure box, and pore water pressure gauge.

The purpose of the test is to observe the law of subgrade settlement and deformation, the distribution and change law of base soil pressure, the change law of soft foundation consolidation, the seasonal change law of groundwater levels, and the change law of stress and deformation distribution of geocells.

The embedded layout of components is shown in Figure 3. The settlement monitor points and earth pressure monitor points are set at the middle and both shoulders of the subgrade. Pore water pressure monitor points are set at the middle of the left-side subgrade. Layered settlement monitor points are set at the middle of the subgrade. The geogrid strain monitor points are set at the geocell of the right-side subgrade.

The test data is collected by the intelligent comprehensive tester JMZX-3001, and the data is collected manually.

Figure 1: Surface water on site.

Table 1: Physical and mechanical properties of bad geological soils in the Hetao area.

Soil name	Silt (0.1 m depth)	Silt (2.1 m depth)	Clay
Sampling depth (m)	0.1	2.2	3.0
Wet density ρ (g/cm^3)	1.91	1.88	1.94
Natural water content w (%)	38.0	24.8	29.5
Dry density ρ_d (g/cm^3)	1.38	1.51	1.50
Proportion G_s	2.70	2.70	2.74
Void ratio n (%)	48.7	44.2	45.3
Void ratio e_0	0.951	0.792	0.829
Saturation S_r (%)	100.0	84.5	97.5
Liquid limit W_L (%)	40.9	40.9	48.5
Plastic limit W_P (%)	31.7	31.9	23.2
Plasticity index I_P	9.2	9.0	25.3
Liquidity index I_L	0.68	-0.79	0.25
Compression factor a (MPa^{-1})	0.242	0.218	0.276
Compression modulus E_s (MPa)	7.936	6.28	6.57
Cohesion c (kPa)	0.35	0.39	7.39
Friction angle φ (°)	30.9	32.9	13.0

The observation frequency is as follows: daily observation is needed when the embankment is under construction, and the number of observations should be increased when filling soil. If there is a long time in the soil filling interval, it can be changed to a two-day or three-day observation. Besides, close attention needs to be paid to the abnormal condition of subgrade settlement. The observation frequency depends on the situation during the embankment preloading period, and it should be measured daily for the first 1~3 months. It can be adjusted to a three-day observation or larger interval along with the stabilization of measured data.

3. Results and Analysis

3.1. Analysis of Layered Settlement. Layered settlement magnetic rings are used to measure the settlements of different soil layers. A hole of 9 m was drilled in the middle of the subgrade, and settlement magnetic rings were set at 2 m intervals, with burial depths of 1, 3, 5, and 7 m, respectively. The test was conducted from October 2016 to September 2017, and the measured data are shown in Figure 3. Due to the extreme weather conditions, the test was suspended for four months from December 2016 to March 2017.

Figure 4 shows the most representative layered settlement-depth distribution curve, as the curves of the five base treatments are very similar. Generally, the maximum value of layered settlement occurs at the ground surface. It is decreasing from the ground surface, but all the curves in this test are in the shape of a bulge. The maximum settlement occurs at 3 m below the surface.

The stratification of ground soil is the leading cause of the bulge-shaped settlement-depth distribution curve. The maximum settlement depth is located at the interlayer of silty clay with a soft plastic state. During the process of subgrade filling construction, the upper load creates additional stress on the ground soil, causing compression soil deformation. There are relatively strong hard shells at the ground surface, in which compression deformation is small, but the soft clay beneath the hard shell is further compressed under additional stress, bringing the settlement magnetic ring to sink. The high underground water level and large water content may cause a horizontal displacement of the soft clay at the surrounding of the subgrade. The fact that the interlayers are compensated by the flowing soft clay does not trigger significant surface settlement.

The development and time of settlement in the middle of the subgrade are shown in Figure 5. It can be seen that settlement increases with the continuous increase of the upper backfill soil. In early November 2016, 0.5 m backfill soil is filled and compacted on the subgrade, and the settlement increases obviously at this moment. After that, the settlement increases slowly. By September 6, 2017, the settlement curve still keeps an increasing trend. The five base treatments are compared, and it was found that the cumulative settlement of the double-layer geogrid scheme is 6.9 cm, which is the smallest among the five schemes until September 6, 2017, followed by the double-layer geocell scheme with a cumulative settlement of 8.7 cm, and the cumulative settlement of the replacement cushion scheme is 9.0 cm,

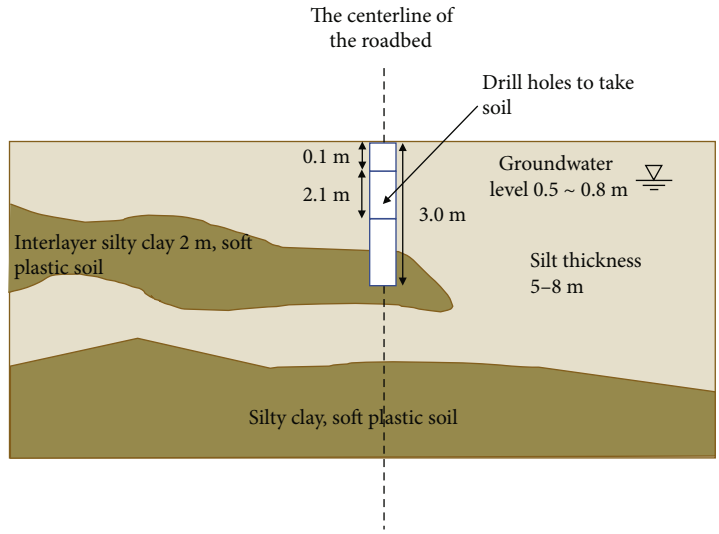

Figure 2: Schematic diagram of soft soil sampling.

Table 2: Experimental section of the subgrade base treatment plan.

The serial number	Treatment plan	Note
Plan 1	Excavation and replacement with 80 cm eolian sand	Layered filling and compacting
Plan 2	Excavation and replacement with 60 cm gravel, reinforcement with the single-layer geocell	The integral-type geocell adopts steel nail insertion, the geocell sheet height is 5 cm, the ultimate tensile strength of the sheet ≥ 160 kN/m, the ultimate tensile strength of the node ≥ 160 kN/m, and the failure elongation ≤ 15%
Plan 3	Replacement with 30 cm gravel, reinforcement with the first-layer geocell, then replacement with 30 cm gravel, reinforcement with the second-layer geocell	
Plan 4	Replacement with 20 cm gravel, reinforcement with the first-layer geogrid, then replacement with 50 cm gravel, reinforcement with the second-layer geogrid	The polypropylene bidirectional geogrid rib width is 22 mm, the mesh size of the geogrid is 140 mm × 140 mm, the longitudinal and transverse ultimate tensile strength ≥ 50 kN/m, the ultimate tensile strength of the node ≥ 500 kN/m, and the failure elongation ≤ 13%
Plan 5	Excavation and replacement with 50 cm gravel, reinforcement with the single-layer geocell	

Table 3: The quantity of embedded sensors in each test section.

Sensors	Plan 1	Plan 2	Plan 3	Plan 4	Plan 5
Earth pressure box	6	6	6	6	6
Flexible displacement meter	/	/	/	4	4
Pore water pressure gauge	2	2	2	2	2
Layered settlement magnetic ring	4	4	4	4	4
Settlement plate	3	3	3	3	3
PVC settling tube	1	1	1	1	1

and the cumulative settlement of the single-layer geogrid scheme is 10.2 cm. The cumulative settlement of the single-layer geocell scheme is 15.4 cm, which is the smallest among the five schemes. Among them, the settlement rate of the single-layer geocell section increases obviously in the later period. The reason may be related to the ground disturbance caused by the excavation of ditches on site. The thicker replacement cushion with the double-layer geocell actually increased the upper load. However, due to the increase of geosynthetics, the ability to disperse the upper load is improved, and the settlement is relatively small with the reduction of additional stress.

The average settlement rates of the five schemes during the construction period differ little from each other, which were 0.2 mm/d, 0.3 mm/d, 0.3 mm/d, 0.3 mm/d, and 0.5 mm/d, respectively. The settlement rate control standard in the relative specification is that the settlement rate of the middle of the subgrade ground should not exceed 10 mm/d. The normal construction requirements for the surface course are that the settlement rate of the subgrade should

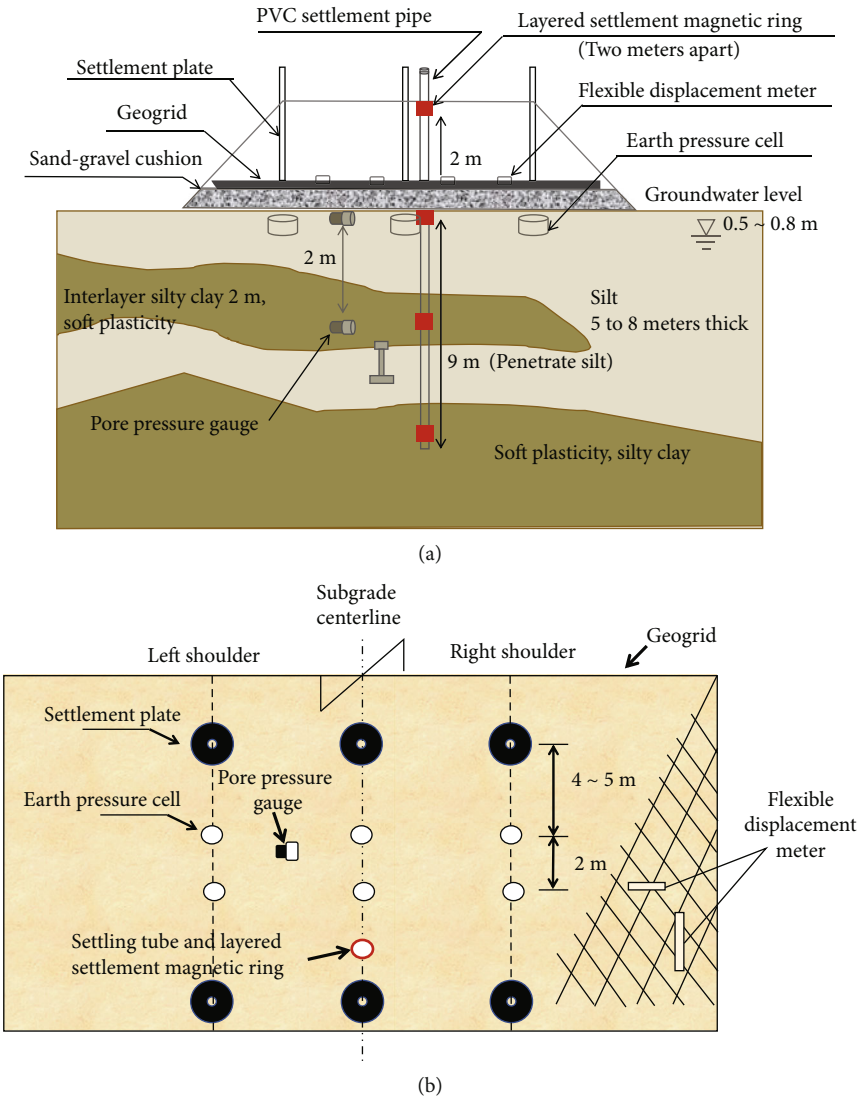

Figure 3: Layout scheme of sensors: (a) layout of the subgrade section and (b) layout of the subgrade planform.

be below 3 mm/d for three consecutive months; it can be seen from the measured data ranging from 0.2 to 0.5 mm/d that all the five experimental sections can meet the requirements. Comprehensive analysis shows that the effect of the double-layer reinforcement to control foundation settlement is better than that of the replacement cushion and single-layer reinforcement. As shown in Figure 5, the difference between the geogrid and the geocell in controlling foundation settlement is not obvious. Therefore, the appropriate reinforcement material can be selected comprehensively, considering the cost and construction speed.

3.2. Analysis of Earth Pressure. The earth pressure boxes are employed to explore the distribution and variation of base earth pressure in different base treatment schemes. Figures 6 and 7 depict the soil pressure-time curve at different positions of the subgrade base. The results show no apparent soil pressure data during the early stages of the subgrade filling construction because of the interference of field machinery equipment and vehicles. The earth pressure increases gradually in the later period. There is a significant fall in soil pressure around mid-October 2016, and the reason is that the farmland irrigation on both sides of the road incurs the rise of the groundwater level and soil water content, and the soil pressure decreases with the increase of buoyancy. When the irrigation period on both sides of the subgrade is finished, the soil pressure gradually recovers and increases. After subgrade filling starts again in May 2017, the earth pressure continues to increase in a steplike manner. Until July, when subgrade filling is completed, the earth pressure gradually tends to be stable. The curve shape changes at each position in the five schemes are basically consistent on the whole.

The comparison of the five treatment schemes shows that the soil pressure of the base at the middle of the subgrade is more significant than that at the shoulder of the subgrade. The subgrade is considered a typical flexible foundation, and the deformation of the subgrade is consistent with that of the ground. In general, the distribution of the base earth pressure is the same as that of the upper load,

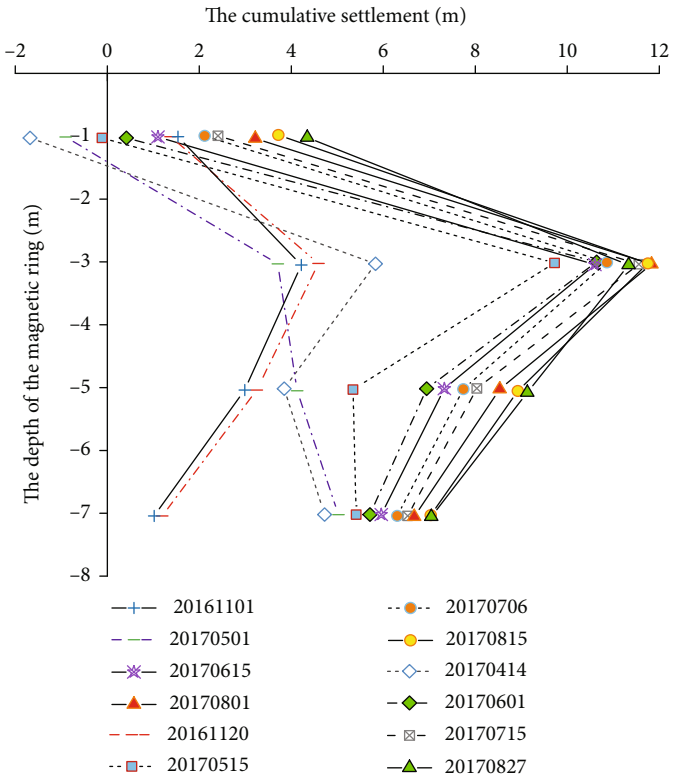

Figure 4: Typical curve of the layered settlement of the subgrade in the experimental section.

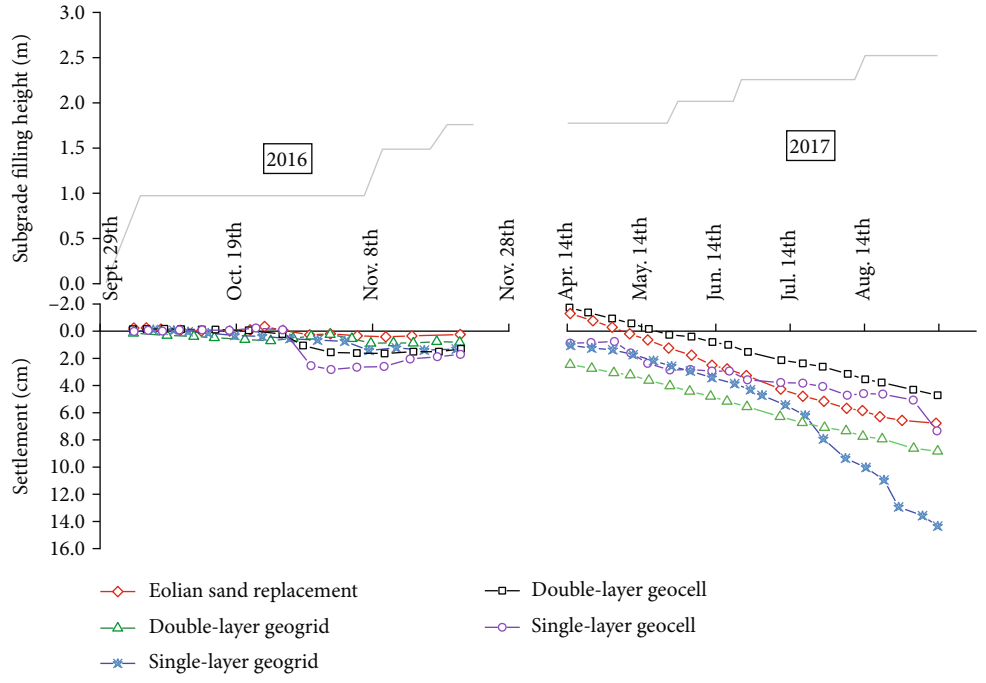

Figure 5: Subgrade middle subsidence-time change curve.

usually presenting a uniform distribution. The obvious large earth pressure in the middle of the test reflects the potential danger of uneven settlement of the subgrade. That is, the disposal effect of the replacement cushion scheme is not well. Using the double-layer geogrid scheme over time, the soil pressure distribution of the base is uniform, indicating that

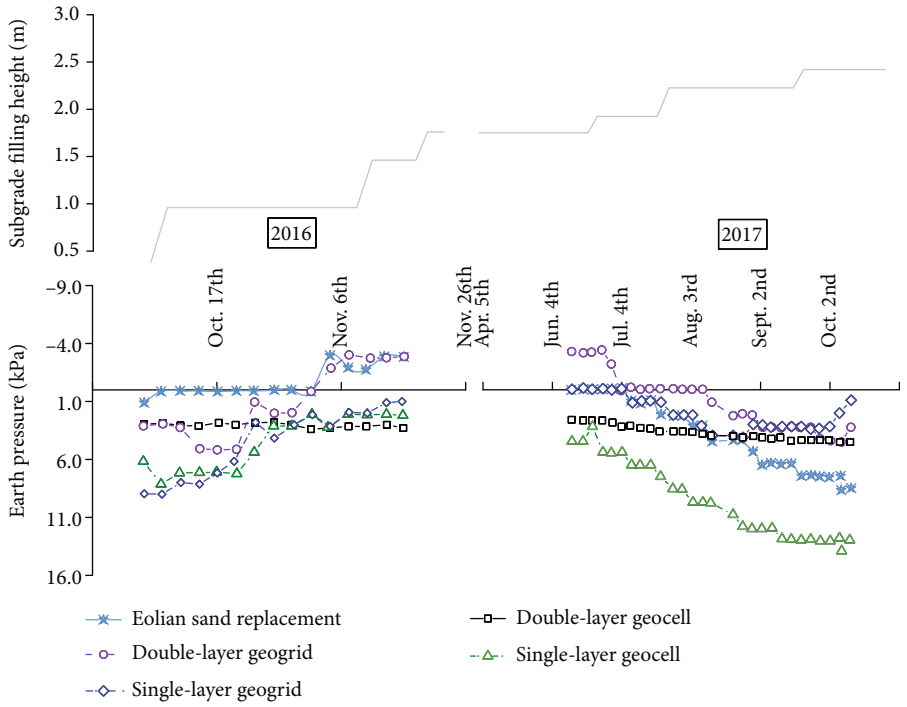

Figure 6: Soil pressure-time curve of the subgrade in the left shoulder base.

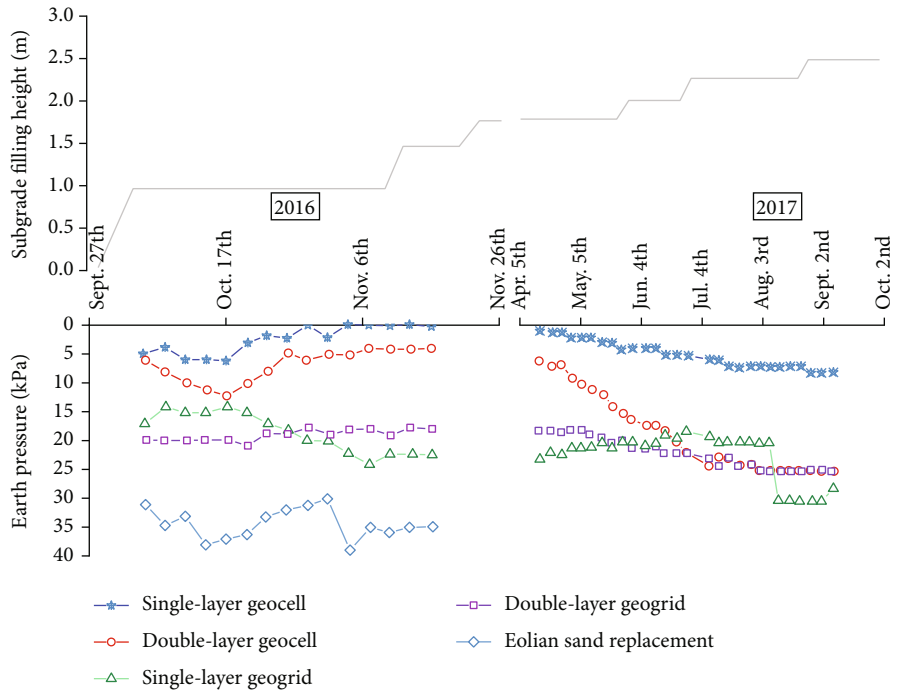

Figure 7: Soil pressure-time curve of the subgrade in the middle part.

when the geogrid is used for reinforcement, the loaded body can play a stress transmission role so that the subgrade stress is relatively uniform.

Figure 7 shows that the average soil pressure value of the base at the middle of the subgrade after stabilization is about 35 kPa, which is consistent with the subgrade filling height of 2.5 m. The average value of soil pressure after stabilization of the single-layer geogrid scheme is 22 kPa, that of the double-layer geogrid scheme is 25 kPa, and that of the double-layer geocell scheme is about 18 kPa. In the mid-October single-floor geocell treatment section, the soil pressure begins to decrease and even becomes negative during irrigation. It

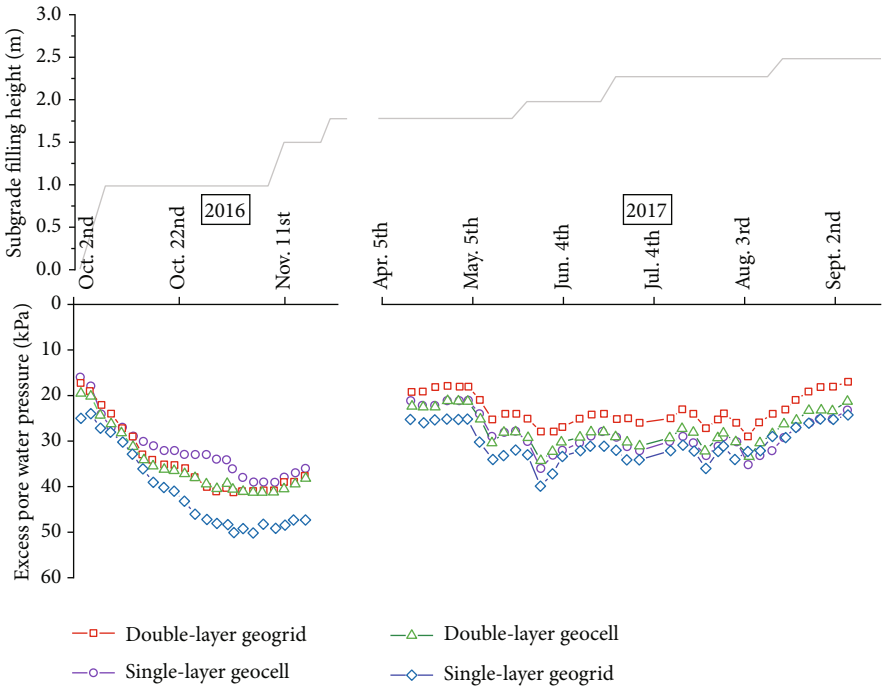

Figure 8: Pore water pressure-time variation curve.

may be due to the fact that there is a lot of water at the test point, and the earth pressure box is affected by the water buoyancy, and its induction plate can feel the change of stress synchronously. After the irrigation period, the soil pressure begins to increase gradually; then, the soil pressure tends to be stable; at this moment, the average value is about 8 kPa.

Comparing the five treatment schemes, it can be seen that the earth pressure value gradually increases over time, and the subgrade stress is smaller than that of the other four when using a single-layer geocell. Comparing Figures 6 and 7, the difference between the soil pressure in the middle of the subgrade and the soil pressure on the shoulder of the road is the smallest in the five treatment schemes; that is, the risk of uneven settlement of the subgrade is low.

3.3. Analysis of Pore Water Pressure. Pore water pressure is divided into hydrostatic pressure, seepage pore water pressure, and excess pore water pressure. Pore water pressure gauges in the test schemes are used for the measurement of pore water pressure. The seepage pore water pressure is the seepage force of the seepage water acting on the soil particles, which is proportional to the hydraulic gradient. In order to figure out the seasonal fluctuation of the groundwater level and surface water caused by seasonal flood irrigation in this area, pore water pressure gauges are set at 4 m below the ground of the subgrade in the middle part of the five experimental sections.

Figure 8 shows the long-term pore pressure variation curve of various treatment schemes, and the pore water pressure increases during the subgrade filling construction and dissipates during the filling construction interval. During the period of farmland irrigation like October 2016 and May 2017, there is a large increase in excess pore water pressure due to the rise in the underground water level. The generation and development of excess pore water pressure can reduce the effective stress acted on soil particles and increase soil deformation; namely, the settlement of the ground enlarges. By August 2017, there was a significant drop in the excess pore water pressure in all sections, indicating that the effective stress gradually increased as the excess pore water pressure dissipated. The pore water seeps from top to bottom of ground soil, the soil consolidates gradually, and the settlement tends to be stable.

3.4. Analysis of Geocell Flexible Displacement. The flexible displacement meters are adopted at the section set geogrids, and a flexible displacement meter is arranged along each layer of the geogrid longitudinally and horizontally, respectively. Four flexible displacement meters are set for the double-layer geogrid in total.

Figures 9 and 10 show the deformation-time variation curve of the geogrid. The trend of deformation in the two sections is basically the same; it stretches and then contracts in both the vertical and horizontal directions. During the subgrade filling construction period, the deformation is positive, and the geogrid is in tension. It may be due to the fact that the settlement of the soil at the measurement point is less than that of the surrounding soil. In the preloading stage, the deformation value decreases and becomes negative gradually, and the geogrid begins to shrink continuously. The deformation trend gradually decreases with time, and the increased rate of negative displacement of the geogrid reduces, indicating that the settlement has tended to be stable. The deformation of the geogrid reflects that the reinforced material has an obvious membrane-pulling effect

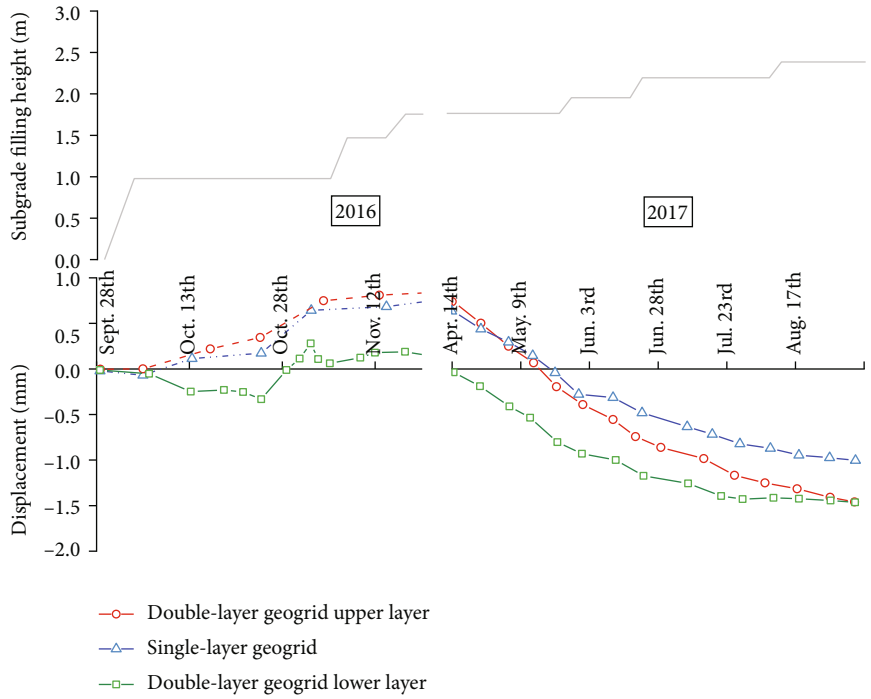

Figure 9: Deformation-time variation curve of the geogrid along the subgrade longitudinal direction.

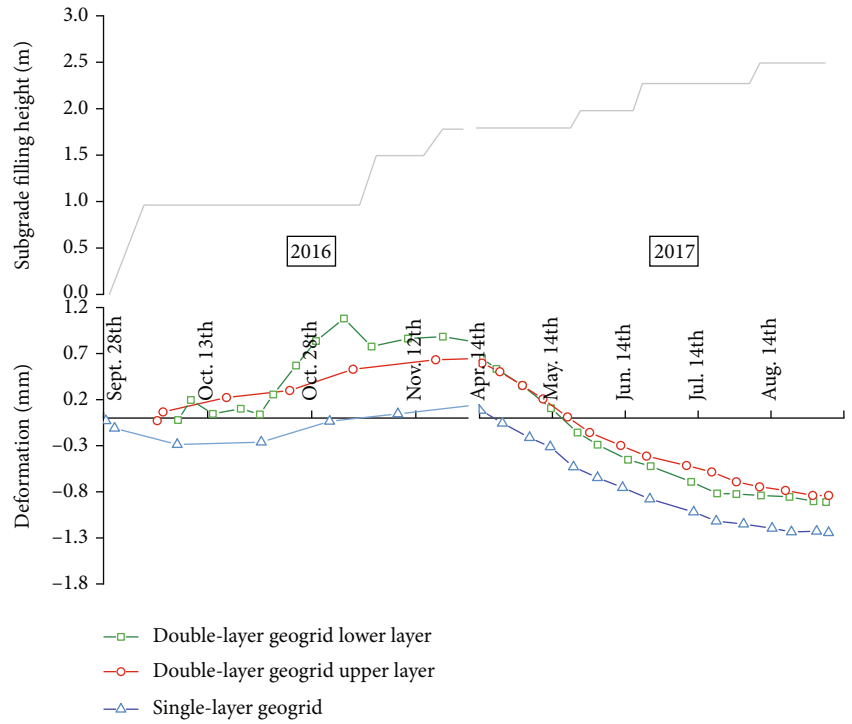

Figure 10: Deformation-time variation curve of the geogrid along the subgrade transverse direction.

during the whole subgrade filling construction. It also indirectly reflects the earth arch effect of subgrade backfill soil.

3.5. Economic Comparison. By comparing the cost of treatment of the cushion material used in the five substrate treatment protocols, the expected economic benefits can be calculated. According to the experimental design scheme, the base treatment of 500 m of the test section was compared, and the treatment costs of each 100 m of the five schemes of replacing the sand and gravel cushion, the

Table 4: Treatment plan economic benefit estimate table.

Treatment scheme	Length	Materials	Dosage (m^3)	Unit price (yuan/m^3)	Cost (ten thousand yuan)
1.0 m gravel slag cushion	100 m	Chip ballast	2800 m^3	80	22.4
Single-layer geogrid	100 m	Geogrid	Geogrid: 2800 m^2	Geogrid: 16	13.7
		Pebbles	Pebbles: 1680 m^3	Pebbles: 55	
Double-layer geogrid	100 m	Geogrid	Geogrid: 5600 m^2	Geogrid: 16	21.3
		Pebbles	Pebbles: 2240 m^3	Pebbles: 55	
Single-layer geocell	100 m	Geocell	Geocell: 2800 m^2	Geocell: 29	17.4
		Pebbles	Pebbles: 1680 m^3	Pebbles: 55	
Double-layer geocell	100 m	Geocell	Geocell: 5600 m^2	Geocell: 29	25.5
		Pebbles	Pebbles: 1680 m^3	Pebbles: 55	

geogrid plus the grit cushion, the double-layer geogrid grit cushion, the geogrid chamber grit cushion, and the double-layer geogrid chamber grit cushion were compared. Among them, the unit price of materials includes ex-factory price, freight, and paving, and the economic assessment data of the five substrate treatment schemes is obtained after analysis and collation, as shown in Table 4.

From the analysis in Table 4, it can be seen that within the range of 500 m in the test section, the costs of the five base treatment plans are in descending order: double-layer geogrid sand-gravel cushion, replacement sand-gravel cushion, double-layer geocell sand-gravel cushion, single-layer geocell sand-gravel cushion, and single-layer geogrid sand-gravel cushion.

4. Conclusion

Relying on the Jingxin Expressway Lin-bai section (Linhe-Baiping) construction project, five subgrade base treatment schemes (eolian sand replacement, single-layer geogrid, double-layer geogrid, single-layer geocell, and double-layer geocell) were employed in the *in situ* test. Based on the long-term subgrade field monitoring, the distribution and variation rules of subgrade layered settlement, earth pressure, pore water pressure, and reinforcement material deformation are obtained and analyzed. Based on the results of the analyzed experimental data, the following conclusions were drawn:

(1) Five subgrade base treatment schemes were used to treat the subgrade, and the postconstruction settlement control all met the requirements of expressway construction specifications. Among them, in the use of double-layer reinforcement control, the foundation settlement is the smallest, achieving the effect of subgrade reinforcement on the soft ground. There is little difference in the settlement control effect between the geocell and the geogrid

(2) Earth pressure and pore water pressure test results demonstrate that agricultural irrigation dramatically increases the groundwater level and incurs ground surface water accumulation, which significantly changes the size and distribution of soil pressure of the subgrade soil

(3) During the subgrade filling construction period, the reinforcement material of the subgrade base has an obvious membrane-pulling effect, which significantly disperses the upper load. Combined with the special hard shell layer of the soft ground in the Hetao area, the overall subgrade settlement can be effectively controlled. Among them, when the single-layer geocell is used, the subgrade stress is smaller than that of the other four, and the risk of uneven settlement is lower

(4) Comparing the economic benefits of the five base treatment schemes, it can be seen that the single-layer geogrid and geocell among the five base treatment schemes have higher economic benefits. Comprehensive data analysis shows that the single-layer reinforcement material has a better effect on the base

Data Availability

Some data, models, or codes generated or used during the study are available from the corresponding authors upon request.

Conflicts of Interest

The authors declare that there are no conflicts of interest regarding the publication of this paper.

Acknowledgments

The authors gratefully acknowledge the financial support of the Key R&D Projects in Shandong Province under Grant number 2019GSF111008, as well as the Natural Science Foundation of Shandong Province under Grant number ZR201702180333.

References

[1] X. Y. Li, S. Y. Zhang, H. Y. Peng, X. Hu, and Y. J. Ma, "Soil water and temperature dynamics in shrub-encroached grasslands and climatic implications: results from Inner Mongolia steppe ecosystem of North China," *Agricultural and Forest Meteorology*, vol. 171-172, pp. 20–30, 2013.

[2] J. Krümmelbein, S. Peth, Y. Zhao, and R. Horn, "Grazing-induced alterations of soil hydraulic properties and functions

in Inner Mongolia, PR China," *Journal of Plant Nutrition and Soil Science*, vol. 172, no. 6, pp. 769–776, 2009.

[3] H. L. Zhao, J. Y. Cui, R. L. Zhou, T. H. Zhang, X. Y. Zhao, and S. Drake, "Soil properties, crop productivity and irrigation effects on five croplands of Inner Mongolia," *Soil and Tillage Research*, vol. 93, no. 2, pp. 346–355, 2007.

[4] K. Li, T. Liang, L. Wang, and Z. Yang, "Contamination and health risk assessment of heavy metals in road dust in Bayan Obo Mining Region in Inner Mongolia, North China," *Journal of Geographical Sciences*, vol. 25, no. 12, pp. 1439–1451, 2015.

[5] S. Tong, "Research on the relationship between economic growth and road traffic infrastructure in Inner Mongolia," *IOP Conference Series: Earth and Environmental Science*, vol. 237, pp. 32135–32135, 2019.

[6] H. W. Zhang, X. Y. Wang, X. Zhao, and P. F. Liu, "In-situ experiment investigations of hydrothermal process of highway in deep seasonal frozen soil regions of Inner Mongolia, China," *Journal of Central South University*, vol. 27, no. 7, pp. 2082–2093, 2020.

[7] W. Leng, Y. Su, J. Teng, R. Nie, and C. Zhao, "Analysis and evaluation on physical characteristics of fine-grained soils prone to mud pumping," *Tiedao Xuebao/Journal of the China Railway Society*, vol. 40, no. 1, pp. 116–122, 2018.

[8] H. Liang, S. Chen, T. Xu, and Y. Ding, "Analysis of foundation deformation in highway extension project of the Inner Mongolia," *Journal of Inner Mongolia Agricultural University (Natural Science Edition)*, vol. 32, no. 2, pp. 216–219, 2011.

[9] Z. Liu, S. An, R. Yuan, and F. Li, "Settlement analysis of soft ground replacement under earthquake," *Applied Mechanics and Materials*, vol. 166, pp. 2379–2382, 2012.

[10] B. Tarawneh, W. A. L. Bodour, A. Shatnawi, and K. Al Ajmi, "Field evaluation and behavior of the soil improved using dynamic replacement," *Case Studies in Construction Materials*, vol. 10, p. e00214, 2019.

[11] H. K. Preetham and S. Nayak, "Geotechnical investigations on marine clay stabilized using granulated blast furnace slag and cement," *International Journal of Geosynthetics and Ground Engineering*, vol. 5, no. 4, pp. 1–12, 2019.

[12] R. Q. Xu, J. H. Li, C. S. Cai, X. G. Li, X. N. Rong, and S. Chang, "Study of strength characteristics of stabilized soil by using stabilizing agent GX08 treating marine and lacustrine soft soil in Hangzhou," *Yantu Lixue/Rock and Soil Mechanics*, vol. 35, no. 6, 2014.

[13] Y. J. Du, N. J. Jiang, S. Y. Liu, S. Horpibulsuk, and A. Arulrajah, "Field evaluation of soft highway subgrade soil stabilized with calcium carbide residue," *Soils and Foundations*, vol. 56, no. 2, pp. 301–314, 2016.

[14] S. Amulya and A. U. Ravi Shankar, "Replacement of conventional base course with stabilized lateritic soil using ground granulated blast furnace slag and alkali solution in the flexible pavement construction," *Indian Geotechnical Journal*, vol. 50, no. 2, pp. 276–288, 2020.

[15] N. J. Jiang, Y. J. Du, S. Y. Liu, M. L. Wei, S. Horpibulsuk, and A. Arulrajah, "Multi-scale laboratory evaluation of the physical, mechanical, and microstructural properties of soft highway subgrade soil stabilized with calcium carbide residue," *Canadian Geotechnical Journal*, vol. 53, no. 3, pp. 373–383, 2016.

[16] Y. Mei, X. Zhang, X. Nong, and L. Fu, "Experimental study of the comprehensive technology of grouting and suspension under an operating railway in the cobble stratum," *Transportation Geotechnics*, vol. 30, p. 100612, 2021.

[17] Y. Guan, X. Cui, D. Huang et al., "Large-scale test of sleeve valve pipe grouted overwet subgrades," *International Journal of Physical Modelling in Geotechnics*, vol. 18, no. 3, pp. 131–145, 2018.

[18] D. Pan, K. Hong, H. Fu, J. Zhou, N. Zhang, and G. Lu, "Influence characteristics and mechanism of fragmental size of broken coal mass on the injection regularity of silica sol grouting," *Construction and Building Materials*, vol. 269, article 121251, 2021.

[19] P. Dongjiang and H. Kairong, "Experimental study of the mechanism of grouting colloidal nano-silica in over-broken coal mass," *Quarterly Journal of Engineering Geology and Hydrogeology*, vol. 54, no. 4, pp. qjegh2020–qjegh2161, 2021.

[20] P. P. He and Z. D. Cui, "Dynamic response of a thawing soil around the tunnel under the vibration load of subway," *Environment and Earth Science*, vol. 73, no. 5, pp. 2473–2482, 2015.

[21] J. Li, Y. Tang, and W. Feng, "Creep behavior of soft clay subjected to artificial freeze–thaw from multiple-scale perspectives," *Acta Geotechnica*, vol. 15, no. 10, pp. 2849–2864, 2020.

[22] C. Zhang, X. Wang, Q. Yan, C. Vipulanandan, and G. Song, "A novel method to monitor soft soil strength development in artificial ground freezing projects based on electromechanical impedance technique: theoretical modeling and experimental validation," *Journal of Intelligent Material Systems and Structures*, vol. 31, no. 12, pp. 1477–1494, 2020.

[23] J. Zhou, W. Zhao, and Y. Tang, "Practical prediction method on frost heave of soft clay in artificial ground freezing with field experiment," *Tunnelling and Underground Space Technology*, vol. 107, p. 103647, 2021.

[24] J. Zhou and Y. Tang, "Practical model of deformation prediction in soft clay after artificial ground freezing under subway low-level cyclic loading," *Tunnelling and Underground Space Technology*, vol. 76, pp. 30–42, 2018.

[25] X. Ou, N. Lyu, T. Li, H. Yin, S. Zhou, and H. Guo, "Study on optimum combination forecasting method for soft soil subgrade settlement in desert area," *Journal of Wuhan University of Technology(Transportation Science & Engineering)*, vol. 41, no. 2, pp. 239–243, 2017.

[26] J. Yang, "Technology research on the treatment of soft subgrade by applying aeolian sand in Hetao area," Hebei University of Technology, 2014.

[27] W. Shan, M. Ma, Y. Guo, and C. Zhang, "Numerical analysis of the influence of block-stone embankment filling height on the water, temperature, and deformation distributions of subgrade in permafrost regions," *Water*, vol. 14, no. 9, p. 1382, 2022.

[28] W. Jiao, "Study of treatment techniques for highway subgrade base on puddle sections in Hetao area," Chang'an University, 2014.

[29] L. Wu, W. Qi, F. Niu, and Y. Niu, "A review of studies on roadbed frozen damage and countermeasures in seasonal frozen ground regions in China," *Journal of Glaciology and Geocryology*, vol. 37, no. 5, pp. 1283–1293, 2015.

[30] P. Jiang, J. Li, S. Zuo, and X. Z. Cui, "Ecological retaining wall for high-steep slopes: a case study in the Ji-Lai Expressway, Eastern China," *Advances in Civil Engineering*, vol. 2020, Article ID 5106397, 13 pages, 2020.

[31] X. Tang, S. M. Stoffels, and A. M. Palomino, "Mechanistic-empirical approach to characterizing permanent deformation of reinforced soft soil subgrade," *Geotextiles and Geomembranes*, vol. 44, no. 3, pp. 429–441, 2016.

[32] W. Zhong, J. Ouyang, D. Yang, X. Wang, Z. Guo, and K. Hu, "Effect of the in situ leaching solution of ion-absorbed rare

earth on the mechanical behavior of basement rock," *Journal of Rock Mechanics and Geotechnical Engineering*, 2021.

[33] H. Wu, G. Zhao, and S. Ma, "Failure behavior of horseshoe-shaped tunnel in hard rock under high stress: phenomenon and mechanisms," *Transactions of Nonferrous Metals Society of China*, vol. 32, no. 2, pp. 639–656, 2022.

[34] M. He, Z. Zzhiqiang, Z. Jiwei, and L. Ning, "Correlation between the constant mi of Hoek-Brown criterion and porosity of intact rock," *Rock Mechanics and Rock Engineering*, vol. 55, no. 2, pp. 923–936, 2022.

[35] X. L. Li, Z. Y. Cao, and Y. L. Xu, "Characteristics and trends of coal mine safety development," *Energy Sources, Part A: Recovery, Utilization, and Environmental Effects*, pp. 1–14, 2020.